Design and optimization of resistive anode for a two-dimensional imaging GEM detector *

Xu-Dong Ju(鞠旭东)[1,2,3;1)] Ming-Yi Dong(董明义)[1,2;2)] Yi-Chen Zhao(赵逸琛)[4]
Chuan-Xing Zhou(周传兴)[1,2,3] Qun Ou-Yang(欧阳群)[1,2]

[1] State Key Laboratory of Particle Detection and Electronics, Beijing 100049, China
[2] Institute of High Energy Physics, Chinese Academy of Sciences, Beijing 100049, China
[3] University of Chinese Academy of Sciences, Beijing 100049, China
[4] Zhengzhou University, Zhengzhou 450001, China

Abstract: A resistive anode for two-dimensional imaging detectors, which consists of a series of high resistivity pads surrounded by low resistivity strips, can provide good spatial resolution while reducing the number of electronics channels required. The optimization of this kind of anode has been studied by both numerical simulations and experimental tests. It is found that to obtain good detector performance, the resistance ratio of the pads to the strips should be larger than 5, the nonuniformity of the pad surface resistivity should be less than 20%, a smaller pad width leads to a smaller spatial resolution, and when the pad width is 6 mm, the spatial resolution (σ) can reach about 105 μm. Based on the study results, a 2-D GEM detector prototype with optimized resistive anode is constructed and a good imaging performance is achieved.

Keywords: resistive anode, GEM, two dimensional detector, spatial resolution, imaging distortion

PACS: 29.40.Cs, 29.40.Gx **DOI:** 10.1088/1674-1137/40/8/086004

1 Introduction

Gas Electron Multipliers (GEMs) [1], an important new type of Micro-Pattern Gaseous Detector (MPGD), have been widely used in particle physics experiments such as CERN-COMPASS [2] because of properties such as good spatial resolution, high count rates, low material budget and so on. Compared to traditional gaseous detectors like drift chambers, the GEM detector has an advantage in the design of its readout electrode, which is separate from the multiplication region, so various readout methods can be used for the GEM detector, such as the 1-D strip, 2-D strip and pixel readout methods [3]. However, these readout methods generally lead to a large number of electronics channels. For example, there are about 30000 channels in the GEM detector of KLOE2 [4]. Therefore, many new readout structures have been developed to reduce the electronics channels.

Based on the four-corner resistive readout method [5, 6], which is widely used in Position Sensitive silicon Detectors (PSD) [7], Sarvestani et al. [8] developed a 2-D interpolating resistive readout structure for Micro-CAT. This readout structure can provide good spatial resolution with an enormous reduction of electronics channels, especially compared to pixel readout. Based on this concept, we developed a triple-GEM detector with 2-D resistive anode [9]. It has been found that the resistive anode has a strong effect on the detector performance. In particular, some resistive anodes lead to serious imaging distortions. To study the effect of the resistive anode, a series of anodes with different parameters have been fabricated and tested. In this paper, the optimization of the resistive anode is studied using both simulations and experiments.

2 Detector setup and simulation model

2.1 Detector setup and principles

The experimental setup is similar to what has been presented in Ref. [9] except that the DAQ system has been changed from CAMAC-Bus to VME-Bus. Figure 1 shows the schematic of the detector setup. Three cascading standard GEM foils from CERN are used as the gas gain device. Electrons generated in the drift region by incoming particles are multiplied in the holes of the GEM foils and then drift to the resistive anode. Charge

Received 25 February 2016, Revised 24 March 2016
∗ Supported by National Natural Science Foundation of China (11375219) and CAS Center for Excellence in Particle Physics (CCEPP)
1) E-mail: juxd@ihep.ac.cn
2) E-mail: dongmy@ihep.ac.cn

induced by electron clouds in the induction region will diffuse on the resistive anode and be collected by the readout nodes at the cell corners. For the detector prototype study, 16 readout nodes covering 3×3 cells were equipped with charge sensitive amplifiers and 12-bit Peak ADCs which were linked to a PC through the VME-bus.

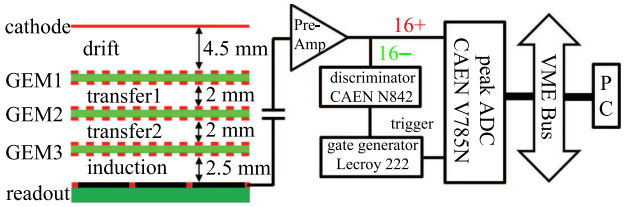

Fig. 1. Schematic of detector setup.

The resistive anode was manufactured by the thick-film resistor process on ceramic board and the structure is shown in Fig. 2. The sensitive area is divided into squared cells. Each cell consists of three parts: the high surface resistivity pad in the cell center, with typical value of 100–1000 kΩ/□, and 7.8 mm×7.8 mm, low surface resistivity strips surrounding the squared pad with typical value of 1–10 kΩ/□ and 8 mm×0.2 mm, and readout nodes at the four corners of the cell.

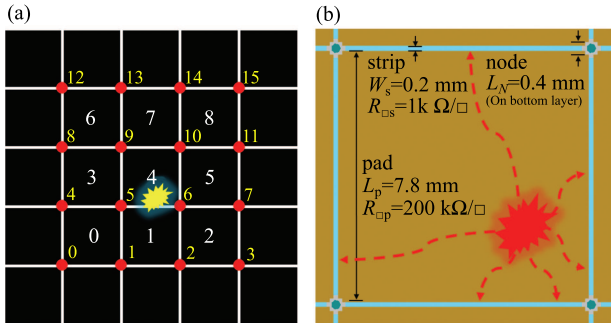

Fig. 2. (color online) (a) Schematic structure of the resistive anode array; (b) Basic resistive anode cell consisting of squared pads with high surface resistivity which are surrounded by strips with low surface resistivity.

The properties of the resistive anode have a determining influence on the detector performance. Considering the structure of the resistive anode in Fig. 2, parameters that may affect the quality of the resistive anode are:

- Resistance ratio of the pad to the strip
- Dimensions of the pad and the strip
- Uniformity of the pad surface resistivity
- ...

A series of resistive anode boards with different parameters have been fabricated to study the influence of the above factors on the detector performance, especially on the spatial resolution.

2.2 Simulation model

In order to understand the mechanics of charge diffusion on the resistive anode as well as to provide a basis for the optimization of the anode structure, a numerical simulation model has been developed [10, 11]. By using the differential Ohm's law,

$$\vec{j}(x,y,t) = -\sigma(x,y)\nabla V(x,y,t) \tag{1}$$

where $\vec{j}(x,y,t)$ represents the wire current density, $\sigma(x,y)$ represents the surface conductivity and $V(x,y,t)$ represents the potential, and the current conservation law,

$$\nabla\cdot\vec{j}(x,y,t)+c\frac{\partial V(x,y,t)}{\partial t}=0 \tag{2}$$

the diffusion equation can be obtained as

$$c\frac{\partial V(x,y,t)}{\partial t}-\nabla\cdot(\sigma(x,y)\nabla V(x,y,t))=I(x,y,t) \tag{3}$$

where $I(x,y,t)$ represents the detector signal induced by electron clouds in the induction region. A simulation using Garfield++ [12] has been developed to evaluate $I(x,y,t)$, which is treated as a space- and time-dependent driving source

$$I(x,y,t)=I_0S(x,y)T(t) \tag{4}$$

and the result is shown in Fig. 3. Therefore, in Eq. (4), the spatial part of the detector signal ($S(x,y)$) is simplified as a Gaussian distribution with σ=0.25 mm, and the time part ($T(t)$) is simplified as a uniform distribution.

The charge diffusion on the resistive anode is then abstracted as the solving of a partial differential equation with the constraint condition that the voltage at all readout nodes equals zero. The explicit finite difference method (FDM) is used to solve the equation in this work [10, 11].

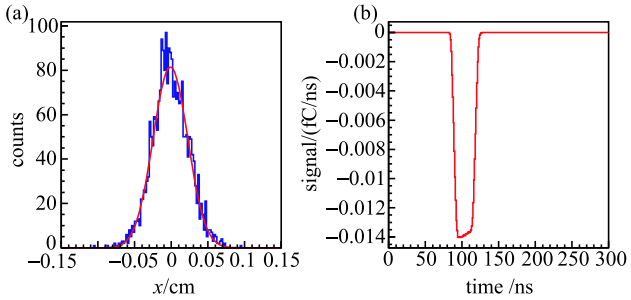

Fig. 3. Garfield++ simulation results of the detector signal. (a) spatial distribution of electrons on the anode in the x-direction; (b) time distribution of charges collected by the anode.

2.3 Reconstruction method

For PSDs, the typical reconstruction method is the charge center of gravity method (COG). Considering the structural characteristics of the 2-D resistive anode readout method, the general reconstruction method is the so-called 4-node-method [7]. It uses the 4 nodes of the fired pad to reconstruct the hit position like

$$X_4 = \frac{\sum_{i=1}^{4} x_i(Q_i - Q_{0i})}{\sum_{i=1}^{4}(Q_i - Q_{0i})} \tag{5}$$

$$Y_4 = \frac{\sum_{i=1}^{4} y_i(Q_i - Q_{0i})}{\sum_{i=1}^{4}(Q_i - Q_{0i})} \tag{6}$$

where x_i and y_i represent the position of the readout nodes, Q_i represents the charge obtained by the electronics system and Q_{0i} represents the baseline of the corresponding readout channel.

To reduce the distortion caused by charge loss from the fired pad to the adjacent pads, some improved methods have been developed [11, 13]. These relatively complex reconstruction methods can lead to good reconstruction results by using more information from the nodes on the adjacent pads.

3 Experiment and simulation results

3.1 Resistance ratio of pad to strip

In the experiments, it is found that the resistance ratio of the pad to the strip seriously affects the detector imaging performance. This ratio is defined as $R_{\square\mathrm{P}}/(R_{\square\mathrm{L}}\cdot N)$, where $R_{\square\mathrm{P}}$ and $R_{\square\mathrm{L}}$ are the surface resistivity of the pad and the strip respectively, and N is the aspect ratio of the strip.

Figure 4 shows the simulation results of different $R_{\square\mathrm{P}}/(R_{\square\mathrm{L}}\cdot N)$. There is pincushion distortion in the imaging results, especially near the edge of the pad, where the distortion is more serious. The main reason is that part of the charge will diffuse across the strip boundary and be collected by neighbouring pads. There is about 40% charge loss (percentage of charge collected by non-fired pads) on the edge of the pad when $R_{\square P} = R_{\square L}$ (Fig. 4 (a)).

On the other hand, from Fig. 4, we also see that the integral distortion becomes less serious with a larger $R_{\square\mathrm{P}}/(R_{\square\mathrm{L}}\cdot N)$. In other words, a larger deviation between the resistance of the pad and the strip can help to improve the detector imaging performance, and when $R_{\square\mathrm{P}}/(R_{\square\mathrm{L}}\cdot N) > 5$, this improvement slows down.

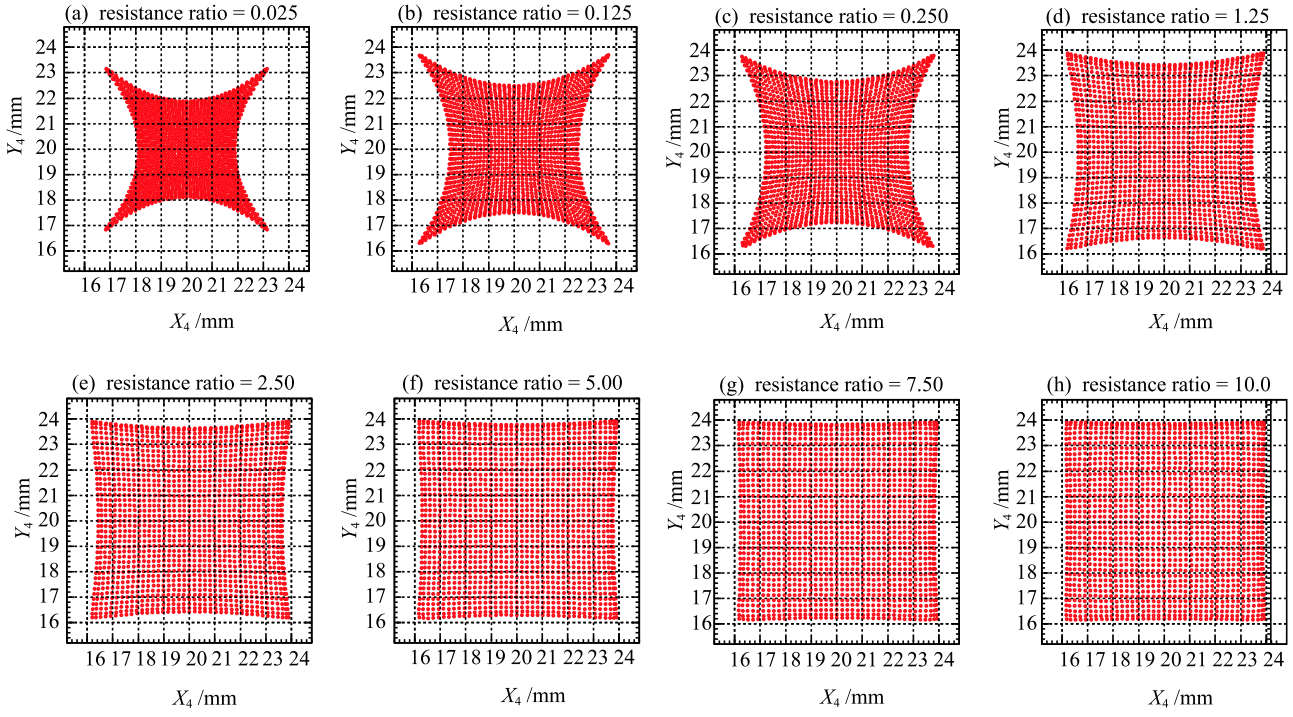

Fig. 4. (color online) Simulation results of different $R_{\square\mathrm{P}}/(R_{\square\mathrm{L}}\cdot N)$. The sizes of the pad and the strip are 8 mm ×8 mm and 8 mm×0.2 mm, respectively. $R_{\square\mathrm{L}}$ is fixed to be 1 kΩ/□, and $R_{\square\mathrm{P}}$ changes from 1 kΩ/□ to 400 kΩ/□ from (a) to (h).

Based on the simulation results, some resistive anodes with different $R_{\square P}/(R_{\square L}\cdot N)$ have been fabricated and tested in a GEM detector. The detector imaging performance is shown in Fig. 5. Compared to the image obtained by using an anode with $R_{\square P}/(R_{\square L}\cdot N)\approx 3$, the pincushion distortion is smaller for that with $R_{\square P}/(R_{\square L}\cdot N)\approx 5$, and this is consistent with the simulation results.

In addition to the influence on the imaging performance, the distortion affects the spatial resolution as well. Figure 6 shows the scan of the spatial resolution (σ, See in Sec. 3.2) of the detector equipped with the corresponding resistive boards in Fig. 5. The spatial resolution decreases from the edge to the middle of a single pad because of the distortion. For a larger $R_{\square P}/(R_{\square L}\cdot N)$, σ is smaller and also much more uniform.

Furthermore, considering the charge diffusion time on the resistive anode, especially for anodes with high surface resistivity [10], a typical range for the surface resistivity of the pad is 100–1000 kΩ/□ and the recommended value of $R_{\square P}/(R_{\square L}\cdot N)$ is larger than 5.

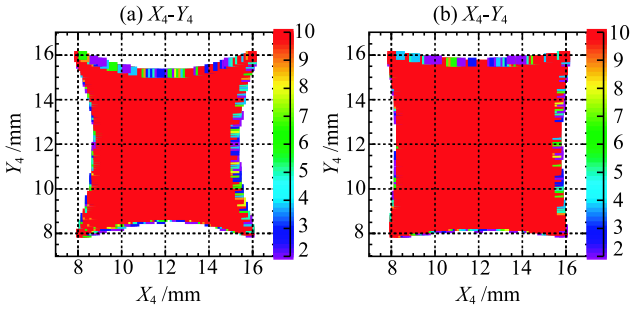

Fig. 5. (color online) The imaging of the detector using resistive anodes with different $R_{\square P}/(R_{\square L}\cdot N)$. The sizes of the pad and the strip are 8 mm×8 mm and 8 mm×0.2 mm, respectively. (a)$R_{\square P}/(R_{\square L}\cdot N)\approx 3$; (b)$R_{\square P}/(R_{\square L}\cdot N)\approx 5$.

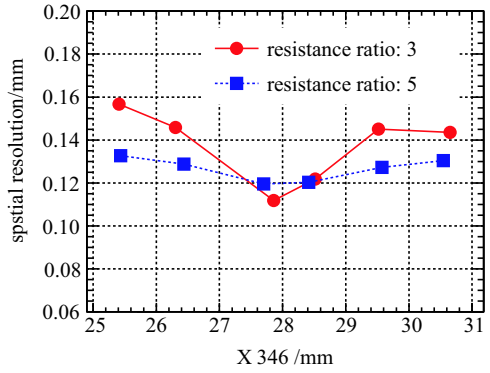

Fig. 6. (color online) Spatial resolution scan of a single pad in 1 mm steps for the resistive anodes in Fig. 5. Results were obtained from a 40 μm slot using an X-ray machine.

3.2 Dimensions of the pad

For the strip and pixel readout methods, the pitch between strips or pixels has a direct effect on the spatial resolution. Accordingly, to study the effect of the pad width on the spatial resolution, resistive anodes with pad dimensions of 6 mm×6 mm, 8 mm×8 mm and 10 mm×10 mm were fabricated and tested. The measurements were made using an X-ray machine with a 40μm slot. A composite 2-gaussian model was used to fit the count distribution as shown in Fig. 7, and the spatial resolution is calculated as

$$\sigma=\sqrt{g\cdot\sigma_{\rm S}^2+(1-g)\cdot\sigma_{\rm B}^2} \tag{7}$$

where σ is the composite spatial resolution, $\sigma_{\rm S}$ is the signal part, $\sigma_{\rm B}$ is the background part, and g is the fraction of the signal [14].

Table 1 shows the spatial resolution of the detector using resistive anodes with different pad width. From Table 1, it can be seen that a better spatial resolution can be obtained by using a smaller pad width. However, for detectors with the same sized resistive anode, a smaller pad width also means slightly more readout channels. Therefore, the selection of the pad width should be a compromise between the spatial resolution and the number of electronics channels, according to the actual application requirements.

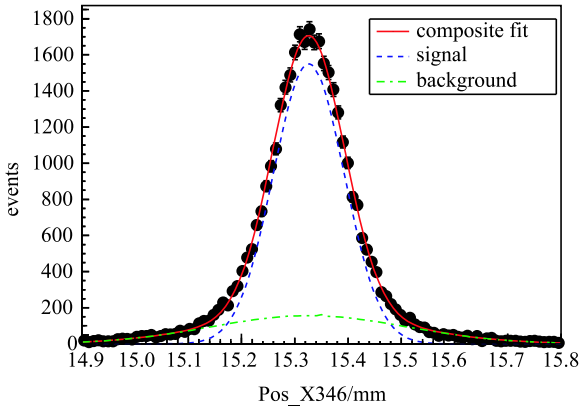

Fig. 7. (color online) Spatial resolution of a detector using a resistive anode with 6 mm×6 mm sized pads. Results were obtained from a 40 μm slot by using an X-ray machine.

Table 1. Spatial resolution with different pad widths.

width/mm	σ/μm	$\sigma_{\rm S}$/μm
6	103.4	66.7
8	112.2	80.0
10	145.1	109.9

3.3 Nonuniformity of the pad surface resistivity

Nonuniformity of the pad surface resistivity is another important factor that can impact on the detector performance. Figure 8 shows the influence of nonuniformity on the imaging performance by simulation. To introduce the nonuniformity effect into the simulation, one single pad is divided into four parts and a constant ratio of the original value of the pad surface resistivity is added to each part. For example, in Fig. 8 (b), +5%, −5%, +5%, −5% of the original value (which means 10% nonuniformity) is added to the corresponding part from left-top to left-bottom in clockwise. From Fig. 8, visual distortion appears when the nonuniformity is larger than 30%, but when the nonuniformity is less than 20%, the deviation is negligible. The nonuniformity effect of the whole board can be obtained by duplicating the single pad to a pad array, and similar simulation results will be acquired.

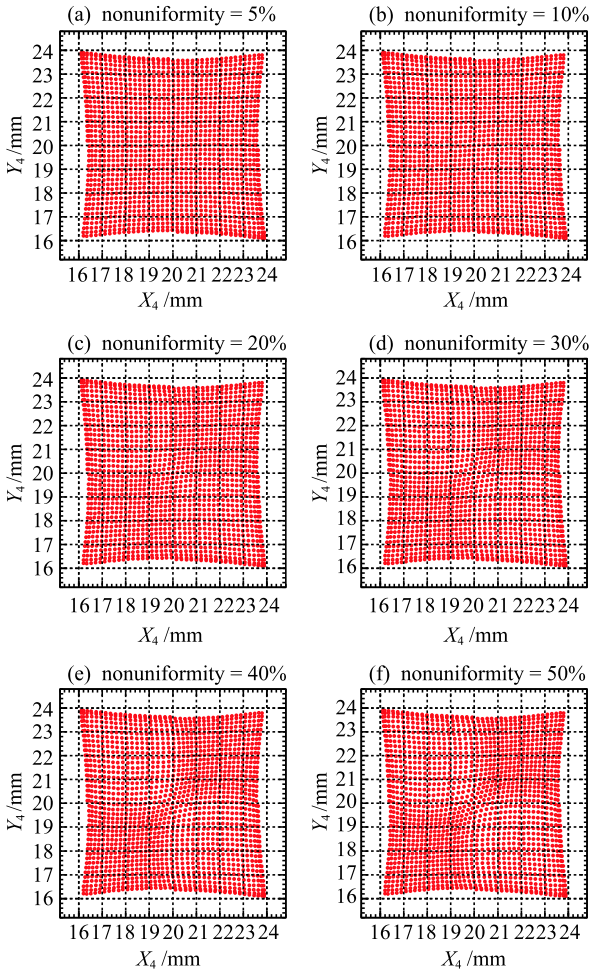

Fig. 8. (color online) Simulation results of nonuniformity of the pad surface resistivity effect on the imaging performance. The sizes of the pad and the strip are 8 mm×8 mm and 8 mm×0.2 mm, respectively. The initial $R_{\square P}$ is 100 kΩ/□ and $R_{\square L}$ is 1 kΩ/□. From (a) to (f), 5%, 10%, 20%, 30%, 40%, 50% deviations respectively are added to the original $R_{\square P}$.

In the experiments, the uniformity of the pad surface resistivity is limited to about 5%–30% by current thick-film resistor technology. The nonuniformity of the resistive board chosen for the GEM detector is required to be less than 20%. In order to study the nonuniformity effect, a scan along the board was carried out. Figure 9 shows the scan result of three pads in 1 mm steps for a board with the nonuniformity of the pad surface resistivity less than 20%. The nonlinearity between the setup position and the measured position is about 1%, which reflects that the board with the nonuniformity of the pad surface resistivity of about 20% has an acceptable influence on the detector performance.

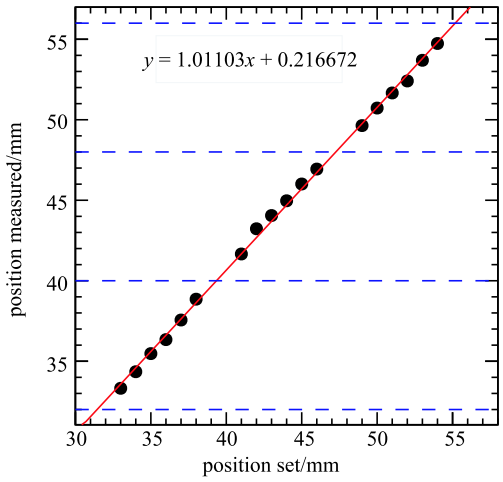

Fig. 9. (color online) Position linearity scan of 3 pads in 1 mm steps. The blue dashed lines represent the edges between neighbouring pads. For this board, the pad size is 8 mm×8 mm and the strip size is 8 mm×0.2 mm, $R_{\square P}/(R_{\square L}\cdot N) \approx 5$ and the nonuniformity of the pad surface resistivity is about 20%. Results were obtained from a 40 μm slot using an X-ray machine.

3.4 Imaging result

Based on the results described above, several optimized resistive anodes were fabricated and tested in a detector prototype with 49 electronics channels. Figure 10 shows the imaging result of a mask "AGE" with slot width of about 1 mm. For this resistive anode board, $R_{\square P}/(R_{\square L}\cdot N) \approx 6$, the pad size is 6 mm×6 mm, the strip size is 6 mm×0.2 mm and the nonuniformity of the pad surface resistivity is less than 20%(Fig. 10). The image was obtained by an X-ray machine 40 cm away from the detector. The image quality is so good that the sharp borders of the letters are detailed. The spatial resolution of the prototype is as good as 103.4 μm (Table 1).

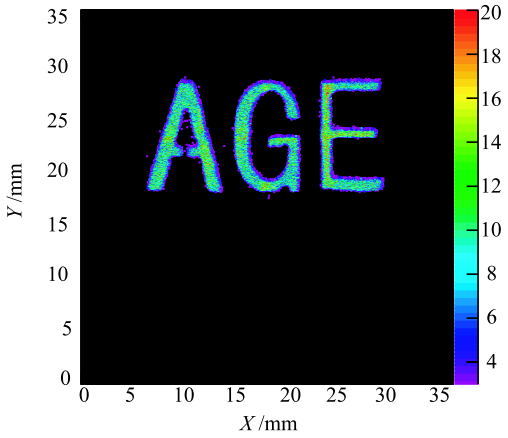

Fig. 10. (color online) Detector imaging of "AGE". The "AGE" pattern, with a typical slot width of about 1 mm and thickness of 12 mm, was printed by a 3D printer.

4 Conclusion

The optimization of the resistive anode has been studied by both experiments and simulations. To obtain good detector performance, the following rules should be considered for the resistive board:

- Resistance ratio of the pad to the strip should be $\geqslant 5$
- Nonuniformity of the pad surface resistivity should be $\leqslant 20\%$
- A smaller pad width leads to a smaller spatial resolution; when the pad width is 6 mm, σ can reach 105 μm.

Besides the factors mentioned above, from experiments, some other factors have been found to contribute to the detector imaging as well. For example, narrower strips benefit the imaging, while current technology limits the strip width to about 0.2 mm. In general, the detector performance results from the combination of the above factors.

This study helps to determine the parameters of resistive readout boards and is enlightening for detectors using similar readout methods. With the spatial resolution about 110 μm, the study also shows the application prospects of the resistive anode readout method in MPGDs.

We wish to express our thanks to Dr. XIU Qing-Lei for the useful discussions and Dr. QI Hui-Rong for the electronics.

References

1 F. Sauli et al, Nucl. Instrum. Methods A, **8**: 386 (1997)
2 D. Abbaneo et al, JINST, **8**: C12031 (2013)
3 F. Thibaud et al, JINST, **9**: C02005 (2014)
4 A. Balla et al, Nucl. Instrum. Methods A, **628**: 194–198 (2011)
5 M. Lampton et al, Review of Scientific Instruments, **50(9)**: 1093–1097 (1979)
6 T. Doke et al, Nucl. Instrum. Methods A, **261**: 605–609 (1987)
7 A. Banu et al, Nucl. Instrum. Methods A, **593**: 399 (2008)
8 A. Sarvestani et al, Nucl. Instrum. Methods A, **419**: 444 (1998)
9 M. Y. Dong et al, Chin. Phys. C, **37(2)**: 026002 (2013)
10 H. Wagner et al, Nucl. Instrum. Methods A, **482**: 334–346 (2002)
11 Q. L. Xiu et al, Chin. Phys. C, **37**: 106002 (2013)
12 http://garfieldpp.web.cern.ch/garfieldpp/documentation/UserGuide.pdf, received 17th May 2015
13 H. Wagner et al, Nucl. Instrum. Methods A, **523**: 287 (2004)
14 L. H. Wu, *Study of the offline calibration for the BESIII drift chamber and the beam test of a prototype*, Ph.D. Thesis(Beijing:Institute of High Energy physics, CAS, 2007)(in Chinese)